Alternating current Josephson effect and resonant superconducting transport through vibrating Nb nanowires

ALEXEI MARCHENKOV*, ZHENTING DAI, BRANDON DONEHOO, ROBERT N. BARNETT AND UZI LANDMAN*

School of Physics, Georgia Institute of Technology, Atlanta, Georgia 30332, USA
*e-mail: alexei.marchenkov@physics.gatech.edu, uzi.landman@physics.gatech.edu

Published online: 22 July 2007; doi:10.1038/nnano.2007.218

In 1962, Josephson made a celebrated prediction: when a constant voltage is applied across a thin insulator separating two superconductors, it will generate an oscillating current[1]. These oscillations are ubiquitous in superconducting weak links of various geometries, and analogues have been found in other macroscopic quantum systems, such as superfluids[2–4] and gaseous Bose-Einstein condensates[5]. The interplay between the oscillating current and external microwave radiation of matching frequency (Shapiro steps[6]) or with internal electrodynamic resonances (Fiske effect[7]) appear as changes in the current–voltage characteristics of superconducting tunnel junctions and provide further insight into the phenomenon. Here, we report measurements and theoretical studies suggesting that Josephson current oscillations interact with atomic-scale mechanical motion as well. We formed a niobium dimer nanowire that acts as a weak link between two superconducting (bulk) niobium electrodes[8]. We find features in the differential conductance through the dimer which we believe correspond to excitations of the dimer vibrational modes by Josephson oscillations and support our results with theoretical simulations.

Josephson current oscillations (and the accompanying electromagnetic radiation) result from the time dependence of the macroscopic quantum phase difference $\Delta\phi$ between two weakly coupled superconductors caused by a constant bias voltage V: $\partial\Delta\phi/\partial t = (2e/h)V$. The phase difference varies linearly in time with a rate determined solely by the applied voltage and fundamental parameters (Planck's constant, h, and the electron charge, e) without any reference to the weak link's geometry or the electronic properties of the superconducting materials. This law is universally applicable to all feasible superconducting coupling structures[9]. Substituting the time-dependent phase into the Josephson d.c. current-phase relation, $I \propto \sin(\Delta\phi)$, gives an oscillatory solution with a frequency $\nu_J = (2e/h)\ V \simeq 483.6 \times 10^{12}\ V$ [Hz]. The charge of $2e$ appearing in this Josephson frequency relation signifies that the a.c. current involves paired electrons (Cooper pairs).

During the last decade, superconducting atomic-size contacts served as a testbed for microscopic treatments of Josephson effects. In this framework, weak links are modelled as normal constrictions sandwiched between superconducting electrodes and having only a few electron transport channels. In the Landauer formalism[10], each channel's conductance is $\tau_j G_0$, where $\tau_j \leq 1$ is the transmission coefficient, and $G_0 = 2e^2/h$ is the conductance quantum. Through the multiple Andreev reflections (MAR) mechanism[11] (Fig. 1b), unpaired electrons, which populate these channels, can traverse constrictions biased by voltages $eV < 2\Delta$ (Δ is the superconducting gap). In each cycle of the MAR 'ladder', a Cooper pair is transferred across a voltage-biased junction. In a weak link, the current is periodic in time, and it can be written as a Fourier series in the Josephson frequency, $\omega_J = 2\pi\nu_J$, and all its n harmonics[12]:

$$I(V,\tau,t) = \sum_n I_n(V,\tau)e^{in\omega_J t}.$$

The above equation contains both dissipative and non-dissipative components. For constrictions whose length is much shorter than the superconducting coherence length, the net d.c. current, $I_{DC}(V, \tau)$, and all the a.c. amplitudes, $I_n(V, \tau)$, can be evaluated numerically[12–14]. This model is remarkably accurate in predicting the current–voltage characteristics of superconducting atomic-size weak links[15–17]. Recently, Josephson oscillations, including higher-order harmonics, were found by studying the Shapiro effect in aluminium atomic contacts[18].

In this report we study the coupling of Josephson oscillations to atomic-scale mechanical motions in niobium superconducting weak links obtained by breaking microfabricated thin-film constrictions[17] in a cryogenic mechanically controlled break junction (MCBJ) setup. Before presenting our results, we summarize our recent findings[8] related to electronic and atomic structure and d.c. superconducting transport properties of Nb nanowires created in the MCBJ. We have reported on experimental and theoretical studies of Nb contacts, when the conductance of which is of the order of $2 - 4G_0$ with a few contributing channels. Although details of the experiments can be found elsewhere[8,17] it is pertinent to note here that our cryogenic MCBJ setup yields remarkably stable contacts and allows high-resolution (with an accuracy of better than 1 pm) reversible manipulation within a 1 Å elongation range. In our previous work, we have identified the appearance of high and

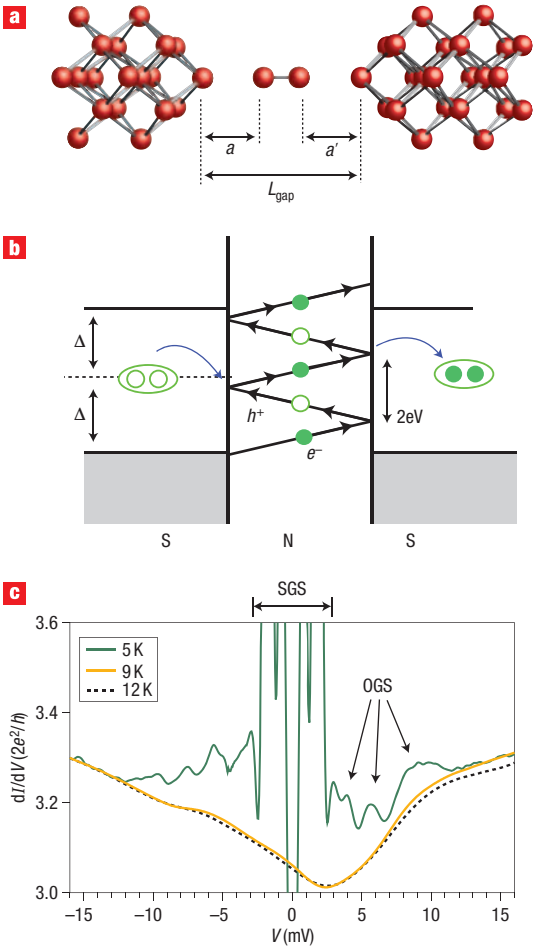

Figure 1 Atomic structure and electronic transport in Nb_2 junctions. a, Symmetric configuration, with the dimer suspended in the middle of the gap between the tips of two crystalline electrodes. **b**, Schematic energy diagram of the multiple Andreev reflection (retro-reflection) process in a ballistic constriction between two superconductors with an energy gap Δ. The electron e^- is retro-reflected as a positively charged hole h^+, creating a Cooper pair in the superconductor; conversely, retro-reflection of a hole annihilates a Cooper pair. Electrons and holes, moving in opposite directions, are both accelerated by the bias voltage V. **c**, Differential conductance curves of a symmetric dimer contact measured below and above the superconducting transition temperature of 8.8 K. In the superconducting state, the low-voltage subgap structure (SGS) is explained by the multiple Andreev reflection model (see Fig. 3). Above the transition temperature, the differential conductance curves are nonlinear owing to backscattering of normal electrons by structural defects in the electrodes and are practically temperature-independent up to at least 12 K. Outside the SGS interval (0 to $\pm$2.5 mV), a series of peaks can be observed for both polarities of the bias voltage. This over-the-gap structure (OGS) disappears in the normal state.

low conductance states. Measurements below and above the superconducting transition temperature allowed determination of the conductance channels, compositions and their dependence on the states of the nanowire. The experimental results were reproduced and explained by density functional theory (DFT) calculations and structure optimizations, coupled with conductance calculations with the non-equilibruim Green's functions (NEGF) technique. In particular, in the DFT calculations, only the distance between the opposing tips is varied, and all the atomic degrees of freedom in the contact region (Fig. 1a) are fully relaxed, and the optimal structure (that is, the lowest energy configuration for a given inter-tip distance) is determined. Following an extensive search that included a number of alternative structures (among them a single atom suspended between the two tips, two tip-apex atoms directly facing each other, and orientationally rotated tips), it has been concluded that at the final stage of elongation before breakup, in the optimal configuration the nanowire consists of a Nb_2 dimer suspended between atomically sharp contacts (Fig. 1a). Depending on the separation, L_{gap}, between the tips, there are two possible equilibrium nanowire configurations: (1) a dimer suspended in the middle of the gap and (2) a state with the dimer's centre of mass shifted towards one of the electrodes. The second, asymmetric, lower-conductance (LG) configuration can be obtained by stretching the first, symmetric, higher-conductance (HG) arrangement. In summary, the nanowire consisting of a suspended Nb_2 dimer has been shown by us to exhibit properties that correlate in a quantitative manner with all the pertinent measurements, including the appearance of a narrow two-level conductance fluctuation region between the HG and LG states[8].

Differential conductance (dI/dV) versus voltage curves for a high-conductance (that is, centred, symmetric) dimer configuration, taken at several temperatures between 4.2 K and 12 K are shown in Fig. 1c and Fig. 2b. These transport characteristics were measured directly using the a.c.-modulated lock-in technique. Below the superconducting transition temperature T_c of our thin-film devices (typically $\sim$8.8 K), we observed both a subgap structure (SGS), manifested as multiple Andreev reflection peaks at voltages $V = 2\Delta/ne$, $n = 1, 2, \ldots$ (see also Fig. 3), and an over-the-gap structure (OGS) consisting of a series of peaks, which are found for both polarities of the bias voltage. Above T_c, both structures disappear, leaving a temperature-independent normal-state base curve (see curves for $T = 9$ K and 12 K in Fig. 1c). The important observations are as follows. (1) Although the SGS peaks shift to lower voltages with increasing temperature following the decreasing superconducting gap $\Delta(T)$, OGS peaks (labelled in Fig. 2b as $l^{\pm}$, $w^{\pm}$, $2l^{\pm}$ and $2w^{\pm}$) do not change their positions. On the other hand, their amplitudes decrease with temperature until they disappear above T_c. (2) The OGS peaks are nearly symmetric at both polarities of the bias voltage; at the lowest temperatures, the peaks l^+ and l^- are obscured by the subgap structure but fully develop when the SGS shifts to lower voltages as the temperature increases (see Fig. 2b).

The existence of the OGS in the dI/dV versus V curves is not governed by the physical mechanism underlying multiple Andreev reflections (which addresses only the SGS spectrum). In our transport experiments OGS peaks were found in 80 contact realizations from six different microfabricated samples, for both high-conductance (symmetric) and low-conductance (asymmetric) dimer contacts. Although the overall characteristics vary slightly for different contact realizations, a similar OGS peak pattern was found in every differential conductance curve. However, no such pattern was observed in either tunnel junctions (when $G < G_0$) or in bulk point contacts (when $G \geq 5G_0$). For such bulk contacts, we commonly observe stepwise drops in the differential conductance at $\sim$16 mV and $\sim$24 mV, which are associated with the onset of longitudinal and transverse phonon modes in the Nb lattice[19] (this is indeed the point-contact spectroscopy regime).

These observations suggest that the aforementioned highly reproducible features in the transport curves originate from atomic-scale structural and dynamical properties of the contact.

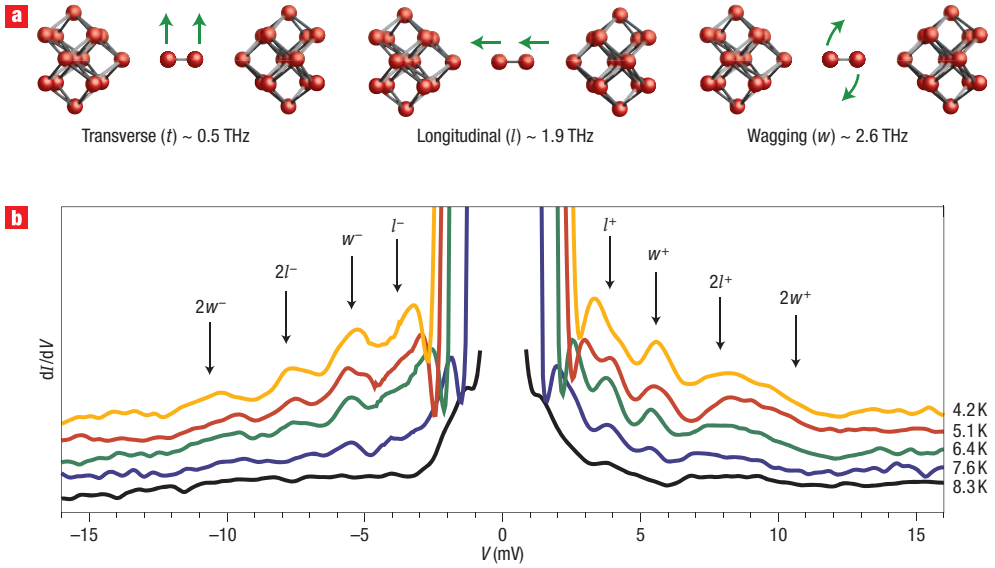

Figure 2 Characterization of dimer vibrational eigenmodes and their interaction with Josephson oscillations. a, Transverse, longitudinal and wagging modes and their eigenfrequencies. **b**, Differential conductance (dI/dV) versus bias voltage measured at different temperatures below the superconducting transition (4.2, 5.1, 6.4, 7.6 and 8.3 K, from top to bottom). The curves are offset for clarity (each by $+0.04G_0$ from the one taken at higher temperature). In addition, in all curves, the subgap structure, with the exception of the dips located just outside of $V = 2\Delta/e \simeq 2.3$ mV, has been removed and the normal-state contribution (that is, the curve taken at 9 K, see Fig. 1c) has been subtracted. Arrows mark the Josephson voltages calculated by substituting dimer vibrational eigenfrequencies into the Josephson frequency relation, and their double values. $l^{\pm}$ labels the longitudinal mode, $w^{\pm}$ labels the wagging mode. Unlike the subgap features, which move with increasing temperature to lower voltages following the gap parameter, labelled peaks' positions do not change as their amplitude decreases. At the lowest temperature of 4.2 K, $l^{\pm}$ peaks are obscured by the subgap structure.

In particular, we propose that the OGS peaks in the superconducting state (which correspond to small current enhancement steps in the current–voltage curves) are caused by resonance coupling between the Josephson current oscillations and the dimer vibrational eigenmodes. The excitation of vibrations by electrons has been observed in most instances with normal metallic electrodes attached to several molecular and nanowire structures, including C_{60} fullerenes[20] and carbon nanotubes[21,22], single-molecule hydrogen and its isotopes[23], single organic molecule junctions and transistors[24,25], and gold atomic chains[26]. In those experiments, vibrational modes were excited, through various mechanisms, by normal electrons travelling through nanoscale constrictions. These vibronic effects occur at voltages $V_n = \hbar\omega_n/e$, where ω_n denotes the frequency of a vibrational mode, and can either enhance or supress the conductance. It is pertinent to remark here that monochromatic bulk phonon generation by a.c. Josephson oscillations has been demonstrated in superconducting tunnel junctions[27] as well as in intrinsic Josephson junctions in high-T_c superconductors[28]. Such effects manifest themselves as changes in the slope of I–V curves, steps in dI/dV versus V records and peaks (dips) in dI/dV or d^2I/dV^2 versus V curves. The exact shape, amplitude and width of these spectroscopic features reflect different vibronic and electronic coupling regimes. The excitation of the vibrational degrees of freedom of nanowires by Josephson current oscillations, described in this paper, is a new process that is intrinsic to superconducting junctions, whose microscopic mechanism may involve the response of atoms in the weak link to the time-dependent electromagnetic field accompanying the a.c. Josephson current.

Bonding of the Nb_2 dimer nanowire to the supporting electrodes mainly involves the Nb d orbitals[8], with the potential energy surface having low curvature along the axis of the constriction and in the direction normal to it. Consequently, the predicted normal-mode eigenfrequencies of the suspended Nb_2 dimer (transverse (t) with eigenfrequency $f_t = 0.5$ THz, longitudinal (l) with $f_l = 1.9$ THz, and wagging (w) with $f_w = 2.6$ THz; see Fig. 2a) are characterized by low frequencies compared with the intradimer stretching frequency (11.1 THz). These frequencies were calculated using first-principles DFT (ref. 8) for the high-conductance state of the symmetric dimer configuration with $L_{gap} = 8.42$ Å and $a = a' = 3.17$ Å (Fig. 1a). The OGS peaks in Fig. 2b correspond to the longitudinal $l^{\pm}$ and wagging $w^{\pm}$ modes; the arrows in this figure indicate (Josephson) voltages obtained by substituting the theoretically predicted eigenfrequencies into the aforementioned Josephson frequency relation. Smaller-amplitude OGS peaks are found in the vicinity of twice the characteristic Josephson voltage values for the longitudinal and wagging modes (marked $2l^{\pm}$ and $2w^{\pm}$ in Fig. 2b). The disappearance of the entire OGS peak spectrum for temperatures above T_c strongly supports the assignment of these latter peaks to coupling between the Josephson current oscillations and second harmonics of the dimer vibrational eigenfrequencies (rather than caused by vibrationally enhanced tunnelling[29]).

Experimental evidence for the existence of Josephson phenomena at frequencies well above the superconducting gap has been demonstrated[30]. Studying the Shapiro effect in Nb point contacts, up to 110 harmonics of a 70 GHz applied signal have been observed, as well as the direct effect of the applied microwave radiation at 2.5 THz. The microscopic theory of Josephson effects in superconducting weak links predicts that at voltages much larger than the superconducting gap, $eV \gg \Delta$, only the first harmonic at the Josephson frequency has a finite amplitude, and all higher harmonics are supressed[12–14].

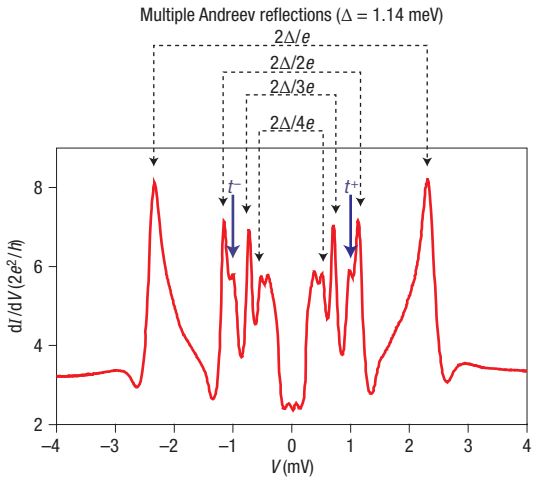

Figure 3 Differential conductance versus voltage measured at 4.2 K in a symmetric dimer contact. The dotted lines indicate multiple Andreev reflection processes of up to the fourth order, which are manifested as peaks at $V = 2\Delta/e$, Δ/e, $2\Delta/3e$ and $2\Delta/4e$. Solid arrows labelled $t^{\pm}$ indicate the Josephson voltage corresponding to the transverse vibrational mode (Fig. 2a).

The dependence of the vibrational frequencies on the elongation of the nanowire has been further explored theoretically. In these calculations, we reduced the separation between the tips from $L_{gap} = 8.42$ Å (Fig. 1a) in the aforementioned configuration to $L_{gap} = 7.73$ Å. Relaxation of this shortened nanowire results in a tilted configuration of the suspended dimer with the Nb–Nb bond forming an angle of $\theta = 27.5^{\circ}$ with respect to the line connecting the apex atoms of the two tips. The normal-mode frequencies determined for this relaxed configuration are $f_t = 0.3$ THz, $f_l = 2.2$ THz, and $f_w = 2.6$ THz. Comparison with the frequencies calculated for a longer nanowire ($L_{gap} = 8.42$ Å) reveals an apparent insensitivity of the vibrational frequencies to the degree of elongation, which reflects the shallow nature of the potential energy surface. We note that larger changes in L_{gap} result in abrupt structural transitions of the nanowire atoms, corresponding to formation of tilted configurations with large tilt angles θ when reducing L_{gap}, or the appearance of highly stretched asymmetric configurations for larger values of L_{gap}, leading eventually to breaking of the contact. These structural transitions are accompanied by electronic conductance and vibrational frequencies that differ significantly from those discussed above. These results correlate with the absence of frequency shifts in our measurements (within our experimental resolution) for contacts whose length was varied by up to 0.6 Å from the configuration for which we show results in this paper. Our experimental resolution is limited by the peaks' widths (about 0.8 mV, which corresponds to ~0.4 THz in terms of the Josephson frequency) and by slight variations in the base curve with elongation.

Evidence for coupling to the transverse mode is shown in Fig. 3. The theoretically predicted frequency of this mode is ~0.5 THz, corresponding to a Josephson voltage of ~1 mV. This value is very close to that of the second-order multiple Andreev reflection peak located at 1.14 mV, which complicates its identification and characterization. Nevertheless, some contacts can be mechanically adjusted so that peaks located at approximately ±1 mV are clearly discernible in the differential conductance curves. In Fig. 3, these peaks are labelled t^{+} and t^{-}; multiple Andreev reflection peaks up to the fourth order are also labelled. The data in Fig. 3 were measured at 4.2 K, because as the temperature increases, the peaks corresponding to the transverse mode become obscured by the shifting subgap structure.

This work proposes and demonstrates that dynamic superconductivity effects can be used to both excite and probe the vibrational degrees of freedom in microscopic objects. For spontaneously formed Nb_2 dimer nanowire junctions[8], we observed features below the superconducting transition temperature, that are consistent with resonant coupling between the a.c. Josephson current oscillations and vibrational eigenmodes of the suspended dimer. Spectral characteristics corresponding to one and two vibrational quanta were measured and found to be in quantitative agreement with the vibrational eigenfrequencies of the suspended dimer as determined from first-principle theoretical calculations. Research of superconducting transport through microscopic objects with intrinsic vibrational degrees of freedom provides a new research avenue. In particular, the details of the microscopic coupling mechanism between the vibrational degrees of freedom in the weak links and the a.c. Josephson currents remain a subject for further experimental and theoretical investigations. Additionally, such systems offer a sensitive spectroscopic method for probing molecular dynamical properties.

Received 3 April 2007; accepted 21 June 2007; published 22 July 2007.

References

1. Josephson, B. D. Possible new effects in superconductive tunnelling. *Phys. Lett.* **1,** 251–253 (1962).
2. Richards, P. L. & Anderson, P. W. Observation of the analog of the ac Josephson effect in superfluid helium. *Phys. Rev. Lett.* **14,** 540–543 (1965).
3. Pereverzev, S. V., Loshak, A., Backhaus, S., Davis, J. C. & Packard, R. E. Quantum oscillations between two weakly coupled reservoirs of superfluid ^{3}He. *Nature* **388,** 449–451 (1997).
4. Hoskinson, E. & Packard, R. E. Thermally driven Josephson oscillations in superfluid ^{4}He. *Phys. Rev. Lett.* **94,** 155303 (2005).
5. Anderson, B. P. & Kasevich, M. A. Macroscopic quantum interference from atomic tunnel arrays. *Science* **282,** 1686–1689 (1998).
6. Shapiro, S. Josephson currents in superconducting tunneling: The effect of microwaves and other observations. *Phys. Rev. Lett.* **11,** 80–82 (1963).
7. Coon, D. D. & Fiske, M. D. Josephson ac and step structure in the supercurrent tunneling characteristic. *Phys. Rev.* **138,** A744–A746 (1965).
8. Marchenkov, A., Dai, Z., Zhang, C., Barnett, R. N. & Landman, U. Atomic dimer shuttling and two-level conductance fluctuations in Nb nanowires. *Phys. Rev. Lett.* **98,** 046802 (2007).
9. Langenberg, D. N., Parker, W. H. & Taylor, B. N. Experimental test of the Josephson frequency-voltage relation. *Phys. Rev.* **150,** 186–188 (1966).
10. Landauer, R. Spatial variation of currents and fields due to localized scatterers in metallic conduction. *IBM J. Res. Dev.* **1,** 223–231 (1957).
11. Klapwijk, T. M., Blonder, G. E. & Tinkham, M. Explanation of subharmonic energy gap structure in superconducting contacts. *Physica B* **109, 110,** 1657–1664 (1982).
12. Averin, D. & Bardas, A. ac Josephson effect in a single quantum channel. *Phys. Rev. Lett.* **75,** 1831–1834 (1995).
13. Cuevas, J. C., Martín-Rodero, A. & Levy Yeyati, A. Hamiltonian approach to the transport properties of superconducting quantum point contacts. *Phys. Rev. B* **54,** 7366–7379 (1996).
14. Bratus', E. N., Shumeiko, V. S., Bezuglyi, E. V. & Wendin, G. dc-current transport and ac Josephson effect in quantum junctions at low voltage. *Phys. Rev. B* **55,** 12666–12677 (1997).
15. Scheer, E., Joyez, P., Esteve, D., Urbina, C. & Devoret, M. H. Conduction channel transmissions of atomic-size aluminum contacts. *Phys. Rev. Lett.* **78,** 3535–3538 (1997).
16. Ludoph, B. *et al.* Multiple Andreev reflection in single atom niobium junctions. *Phys. Rev. B* **61,** 8561–8569 (2000).
17. Dai, Z. & Marchenkov, A. Subgap structure in resistively shunted superconducting atomic point contacts. *Appl. Phys. Lett.* **88,** 203120 (2006).
18. Chauvin, M. *et al.* Superconducting atomic contacts under microwave irradiation. *Phys. Rev. Lett.* **97,** 067006 (2006).
19. Naidyuk, Y. G. & Yanson, I. K. *Point-Contact Spectroscopy* (Springer, New York, 2004).
20. Park, H. *et al.* Nanomechanical oscillations in a single C_{60} transistor. *Nature* **407,** 57 (2000).
21. Sazonova, V. *et al.* A tunable carbon nanotube electromechanical oscillator. *Nature* **431,** 284–287 (2004).
22. LeRoy, B. J., Lemay, S. G., Kong, J. & Dekker, C. Electrical generation and absorption of phonons in carbon nanotubes. *Nature* **432,** 371–374 (2004).
23. Smit, R. H. M. *et al.* Measurement of the conductance of a hydrogen molecule. *Nature* **419,** 906–909 (2002).
24. Stipe, B. C., Rezaei, M. A. & Ho, W. Single-molecule vibrational spectroscopy and microscopy. *Science* **280,** 1732–1735 (1998).
25. Zhitenev, N. B., Meng, H. & Bao, Z. Conductance of small molecular junctions. *Phys. Rev. Lett.* **88,** 226801 (2002).
26. Agraït, N., Untiedt, C., Rubio-Bollinger, G. & Vieira, S. Onset of dissipation in ballistic atomic wires. *Phys. Rev. Lett.* **88,** 216803 (2002).
27. Berberich, P., Buemann, R. & Kinder, H. Monochromatic phonon generation by the Josephson effect. *Phys. Rev. Lett.* **49,** 1500–1503 (1982).

28. Schlenga, K. *et al.* Subgap structures in intrinsic Josephson junctions of $Tl_2Ba_2Ca_2Cu_3O_{10+\delta}$ and $Bi_2Sr_2CaCu_2O_{8+\delta}$. *Phys. Rev. Lett.* **76,** 4943–4946 (1996).
29. Koch, J., Semmelchak, M., von Oppen, F. & Nitzan, A. Current-induced nonequilibrium vibrations in single-molecule devices. *Phys. Rev. B* **73,** 155306 (2006).
30. McDonald, D. G., Evenson, K. M., Wells, J. S. & Cupp, J. D. High-frequency limit of the Josephson effect. *J. Appl. Phys.* **42,** 179–181 (1971).

Acknowledgements

This research was supported by the Georgia Institute of Technology through the Nanoscience/Nanoengineering Research Program (NNRP) and the US National Science Foundation CAREER grant no. DMR-0349110 (Z.D., B.D. and A.M.). The work of R.N.B. and U.L. is supported by the US Department of Energy.
Correspondence and requests for materials should be addressed to A.M. and U.L.
Supplementary information accompanies this paper on www.nature.com/naturenanotechnology.

Competing financial interests

The authors declare no competing financial interests.